Physica A 449 (2016) 74–84

Contents lists available at ScienceDirect

Physica A

journal homepage: www.elsevier.com/locate/physa

Modeling transport through an environment crowded by a mixture of obstacles of different shapes and sizes

Adam J. Ellery [a], Ruth E. Baker [b], Scott W. McCue [a], Matthew J. Simpson [a,*]

[a] School of Mathematical Sciences, Queensland University of Technology, Brisbane, Australia

[b] Mathematical Institute, University of Oxford, Radcliffe Observatory Quarter, Woodstock Road, Oxford, UK

HIGHLIGHTS

- Stochastic simulations of individual and collective motion through a crowded environment.
- Crowded environments populated by mixtures of obstacles of different shapes and sizes.
- Transport properties depend on the obstacle volume fraction and details of the obstacle shape and size distribution.
- Standard fractional diffusion equation descriptions ought to be used with care.

ARTICLE INFO

Article history:
Received 2 July 2015
Received in revised form 17 November 2015
Available online 6 January 2016

Keywords:
Random walk
Crowded transport
Fractional diffusion equation
Diffusion
Hindered transport

ABSTRACT

Many biological environments are crowded by macromolecules, organelles and cells which can impede the transport of other cells and molecules. Previous studies have sought to describe these effects using either random walk models or fractional order diffusion equations. Here we examine the transport of both a single agent and a population of agents through an environment containing obstacles of varying size and shape, whose relative densities are drawn from a specified distribution. Our simulation results for a single agent indicate that smaller obstacles are more effective at retarding transport than larger obstacles; these findings are consistent with our simulations of the collective motion of populations of agents. In an attempt to explore whether these kinds of stochastic random walk simulations can be described using a fractional order diffusion equation framework, we calibrate the solution of such a differential equation to our averaged agent density information. Our approach suggests that these kinds of commonly used differential equation models ought to be used with care since we are unable to match the solution of a fractional order diffusion equation to our data in a consistent fashion over a finite time period.

© 2016 Elsevier B.V. All rights reserved.

1. Introduction

Many biological environments, such as those shown in Fig. 1(a)–(b), are crowded by macromolecules, organelles and cells of varying size and shape. Experimental and computational evidence suggests that crowding effects may impede the transport of macromolecules and cells in such environments [1–7]. Therefore, the development of reliable mathematical models of this transport process is very important. Several previous studies have sought to describe crowded transport processes using either random walk simulation models [8–18] or fractional order diffusion equation (FDE) models [19–29].

* Corresponding author.
E-mail address: matthew.simpson@qut.edu.au (M.J. Simpson).

http://dx.doi.org/10.1016/j.physa.2015.12.123
0378-4371/© 2016 Elsevier B.V. All rights reserved.

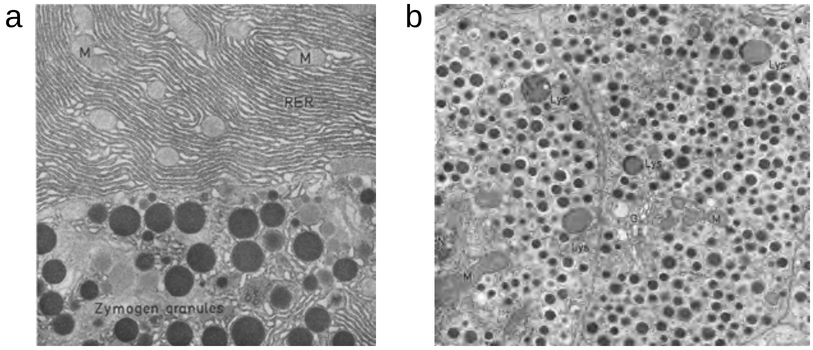

Fig. 1. (a) Intracellular image of mouse pancreatic acinar cells [34]. (b) Intracellular image of alpha cells from a diabetic mouse [34]. Images (a)–(b) are reproduced with kind permission from Springer.

Although some previous studies have considered the effect of different obstacle shapes and sizes in detail [30–33], others have simply focused on studying transport through environments in which a single type of obstacle is present [14,15]. Here, we focus on environments containing a mixture of different types of obstacles since experimental images (Fig. 1(a)–(b)) indicate that many biological environments contain multiple types of obstacles, whose sizes vary considerably.

In this work, we examine the transport of both individual agents and populations of agents through crowded environments using a lattice-based unbiased nearest neighbor random walk model. We simulate crowding effects by randomly populating the lattice with immobile obstacles of different shapes and sizes, whose relative densities are specified by a particular distribution. By holding the density of lattice sites occupied by obstacles, ϕ, constant, and varying the relative density of each individual obstacle type, we are able to create different crowding environments. Some of these environments are dominated by small obstacles, whilst others are dominated by large obstacles.

Although the idea of studying transport through a crowded environment using random walk simulations has become well-established since Saxton's original studies over twenty years ago [12,13], this area of research remains active with many recent studies making valuable contributions. For example, recent theoretical advancements have extended Saxton's lattice-based results to lattice-free frameworks [30,35,36], including studying the role of obstacle orientation [37]. Progress has also been made by combining experimental and theoretical approaches, for example, studying overlapping circular and elliptical obstacles [38] and studying more complicated environments containing up to 15 different types of obstacles [31]. Other more experimentally oriented studies have sought to interpret trajectory data describing the motion of individual cells or molecules using various mathematical frameworks [32,33,39].

In addition to this collection of studies which explicitly focus on motion through crowded environments, other researchers have made progress towards the development, application and solution of FDE models that are thought to implicitly represent crowded transport. Such FDE models have been analyzed in various biological settings including chemical reactions [23], reaction fronts [22,24] and reaction–diffusion mechanisms [25]. We would like to emphasize that the group of studies described here, focusing explicitly on motion through crowded environments using experimental and simulation data [30–33,35–39], have not attempted to interpret their results using any kind of FDE framework. Conversely, the group of studies described here focusing on FDE models [21–25] have not attempted to connect the solution of any FDE model to measurements from any simulation or experiment which explicitly represents transport through a crowded environment. Therefore, given the discrepancy between these two active areas of the literature, one of the aims of the present study is to consider a stochastic model of transport through a crowded environment containing a mixture of different obstacle shapes and sizes and to use averaged data from the stochastic model to examine whether it is possible to represent the transport process using a simpler FDE framework. Although there is a current debate in the literature about how to discriminate between obstructed diffusion, CTRWs and FDEs, and fractional Brownian motion [40], we concentrate on CTRWs and FDEs in this work.

2. Stochastic simulations

We consider a two-dimensional square lattice, with lattice spacing Δ, where we index sites (i, j), with $0 \le i \le M$ and $0 \le j \le N$, so that each site has location $(x, y) = (i\Delta, j\Delta)$. The dimension of the lattice is $0 \le x \le L_x$ and $0 \le y \le L_y$, where $L_x = (M + 1)\Delta$ and $L_y = (N + 1)\Delta$. At the start of a simulation we randomly populate the lattice with immobile obstacles to a specified, spatially uniform density, ϕ. We then place either a single motile agent (Section 3) or a population of motile agents (Section 4) on vacant sites. These agents undergo an unbiased nearest neighbor random walk in which we enforce a simple exclusion condition [41]. Potential motility events that would lead to an agent occupying the same site as another agent or an obstacle are aborted. We use the Gillespie algorithm [42] to advance the simulation until we reach some time T. We always average our results over K identically prepared realizations. The initial location of the motile agent is randomly chosen in each realization. To minimize the computational expense, we regenerate the obstacle field every R

realizations [11,14]. Provided that R is sufficiently small, this has no observable effect on the averaged results [11,14]. For all results presented we always checked that the results were insensitive to the size of the lattice.

In this study, we consider four types of obstacles which occupy the following: (i) a single lattice site (1×1); (ii) two adjacent lattice sites (1×2); (iii) four lattice sites in a square arrangement (2×2); and (iv) nine lattice sites in a square arrangement (3×3). We note that 1×1, 2×2 and 3×3 obstacles are symmetric with respect to the lattice whilst 1×2 obstacles are not. When placing the asymmetric 1×2 obstacles on the lattice, we always take care to randomly orient the obstacles so that, on average, there is no preferred direction of alignment.

For any distribution of obstacles placed on the lattice at random, the total area occupied by the obstacles is approximately given by $\sum_m A_m n_m = \lfloor NM\phi \rfloor$, where A_m denotes the area of the mth obstacle type, n_m denotes the number of the mth obstacle type, $\lfloor \cdot \rfloor$ denotes the floor function and the sum is taken over all obstacle types considered. Although this relationship is an approximation, we find that $\sum_m A_m n_m - \lfloor NM\phi \rfloor$ is extremely small provided that we consider a sufficiently large lattice, which means that the approximation is very accurate and does not impact our results. For example, for all choices of M, N and ϕ used in this work, we find that $\sum_m A_m n_m - \lfloor NM\phi \rfloor < 3 \times 10^{-5}$. Here we use the floor function because in any stochastic realization of the model, the summation is always an integer, whereas $NM\phi$ is not always an integer.

In all cases that we consider, with four types of obstacles, we have

$$n_{(i)} + 2n_{(ii)} + 4n_{(iii)} + 9n_{(iv)} = \lfloor NM\phi \rfloor, \tag{1}$$

where we have expanded the sum and substituted the size of each obstacle into the equation. Since Eq. (1) is Diophantine [43] with four unknowns, it is necessary to enforce some additional relationships between the different types of obstacles to ensure that the solution is unique. In particular, we consider three different situations:

I. *Decreasing distribution:* A distribution in which the number of lattice sites occupied by each type of obstacle forms a decreasing geometric series, in which smaller obstacles are more abundant than larger obstacles. In this case, the ratio of the number of sites occupied by each successive type of obstacle is a positive constant, r. Mathematically, we can write this as $(A_{(i)}n_{(i)})/(A_{(ii)}n_{(ii)}) = (A_{(ii)}n_{(ii)})/(A_{(iii)}n_{(iii)}) = (A_{(iii)}n_{(iii)})/(A_{(iv)}n_{(iv)}) = r$. To solve explicitly for the number of each obstacle type, we note that

$$\begin{aligned} A_{(i)}n_{(i)} &= r^3 A_{(iv)}n_{(iv)}, \\ A_{(ii)}n_{(ii)} &= r^2 A_{(iv)}n_{(iv)}, \\ A_{(iii)}n_{(iii)} &= r A_{(iv)}n_{(iv)}. \end{aligned} \tag{2}$$

Substituting Eqs. (2) into Eq. (1) gives

$$A_{(iv)}n_{(iv)} \left(1 + r + r^2 + r^3\right) = \lfloor NM\phi \rfloor. \tag{3}$$

Finally, combining the solution of Eq. (3) with Eqs. (2) gives

$$\begin{aligned} n_{(i)} &= \frac{r^3 \lfloor NM\phi \rfloor}{A_{(i)}\beta}, \qquad n_{(ii)} = \frac{r^2 \lfloor NM\phi \rfloor}{A_{(ii)}\beta}, \\ n_{(iii)} &= \frac{r \lfloor NM\phi \rfloor}{A_{(iii)}\beta}, \qquad n_{(iv)} = \frac{\lfloor NM\phi \rfloor}{A_{(iv)}\beta}, \end{aligned} \tag{4}$$

where $\beta = 1 + r + r^2 + r^3$. When the coefficients in Eqs. (4) are non-integers we apply the floor function. Choosing $r = 4$, and substituting the values for $A_{(m)}$ for each case, we obtain

$$\begin{aligned} n_{(i)} &= \frac{576}{765} \lfloor NM\phi \rfloor, \qquad n_{(ii)} = \frac{72}{765} \lfloor NM\phi \rfloor, \\ n_{(iii)} &= \frac{9}{765} \lfloor NM\phi \rfloor, \qquad n_{(iv)} = \frac{1}{765} \lfloor NM\phi \rfloor. \end{aligned} \tag{5}$$

The coefficients in Eqs. (5) determine the number of occupied lattice sites for each obstacle type. As expected, the number of lattice sites occupied by smaller 1×1 obstacles is much greater than the number occupied by larger 3×3 obstacles.

II. *Increasing distribution:* A distribution in which larger obstacles are more abundant than smaller obstacles. In this case we assume that the number of 1×1, 1×2, 2×2 and 3×3 obstacles form the first, second, fourth and ninth terms in an increasing geometric series in which the ratio between successive terms is r. These terms are chosen to coincide with the area of each obstacle type. It follows that

$$\begin{aligned} n_{(ii)} &= r\, n_{(i)}, \\ n_{(iii)} &= r^3\, n_{(i)}, \\ n_{(iv)} &= r^8\, n_{(i)}. \end{aligned} \tag{6}$$

The solution of Eq. (1) with Eqs. (6) is

$$n_{(i)} = \frac{\lfloor NM\phi \rfloor}{\gamma}, \qquad n_{(ii)} = \frac{r\lfloor NM\phi \rfloor}{\gamma},$$
$$n_{(iii)} = \frac{r^3\lfloor NM\phi \rfloor}{\gamma}, \qquad n_{(iv)} = \frac{r^8\lfloor NM\phi \rfloor}{\gamma}, \tag{7}$$

where $\gamma = 1 + 2r + 4r^3 + 9r^8$. In our case, choosing $r = 5/4$, we have

$$n_{(i)} = \frac{65536}{4257001}\lfloor NM\phi \rfloor, \qquad n_{(ii)} = \frac{81920}{4257001}\lfloor NM\phi \rfloor,$$
$$n_{(iii)} = \frac{128000}{4257001}\lfloor NM\phi \rfloor, \qquad n_{(iv)} = \frac{390625}{4257001}\lfloor NM\phi \rfloor. \tag{8}$$

As expected, the number of larger 3×3 obstacles is much greater than the number of smaller 1×1 obstacles.

III. *Constant distribution:* A distribution in which the number of lattice sites occupied by each type of obstacle is equal: $n_{(i)} = 2n_{(ii)} = 4n_{(iii)} = 9n_{(iv)}$. The solution of Eq. (1) with this condition is given by

$$n_{(i)} = \frac{36}{144}\lfloor NM\phi \rfloor, \qquad n_{(ii)} = \frac{8}{144}\lfloor NM\phi \rfloor,$$
$$n_{(iii)} = \frac{9}{144}\lfloor NM\phi \rfloor, \qquad n_{(iv)} = \frac{4}{144}\lfloor NM\phi \rfloor. \tag{9}$$

In this case, no obstacle type occupies a larger proportion of lattice sites than any other. Distribution III is an intermediate case relative to distributions I and II, and we refer to distributions I, II and III as decreasing, increasing and constant distributions, respectively.

In Fig. 2(a)–(c) we show the proportion of lattice sites occupied by each obstacle type for $\phi = 0.2, 0.3$ and 0.4, respectively. Specifically, in each subfigure, we show the relative density of occupied lattice sites, $\phi_m = A_{(m)}n_{(m)}/(\lfloor NM\phi \rfloor)$, for each obstacle type. For each value of ϕ shown, the decreasing distribution has a relative abundance of small obstacles, the increasing distribution has a relative abundance of large obstacles, and the constant distribution lies between. Fig. 2(d)–(f) show lattices occupied by obstacles from the decreasing, increasing and constant distributions, respectively. Visually, in Fig. 2(e), which shows a lattice occupied by obstacles drawn from an increasing distribution, we see that the crowded environment contains many vacant, interconnected and spacious corridors. Conversely, Fig. 2(d), which shows a lattice occupied by obstacles drawn from the decreasing distribution, appears to contain far less of these vacant interconnected corridors. Fig. 2(f), which corresponds to the constant distribution, lies between these two cases. Therefore, in summary, visual inspection of the different crowding environments indicate that a lattice crowded using the increasing distribution appears to contain the highest degree of interconnected free space which we anticipate will facilitate transport more readily than the decreasing or constant lattice environments. We note that while it might be straightforward to anticipate this qualitative trend, it is not, by any means, obvious what the quantitative differences between transport through these different environments might be. In Sections 3 and 4 we attempt to apply mathematical models to describe motion through these different environments in order to provide such quantitative information.

To be consistent with previous simulation studies we take care to ensure that ϕ is always less than the site percolation threshold [14,16,17] which, for a square lattice occupied by 1×1 obstacles, is approximately 0.5927 [41]. We also note that visual inspection of the crowding environments in Fig. 2 confirms the presence of closed regions of free space. If we consider a random walk within such a crowded environment, with a motile agent being placed in such a closed region, then the agent will remain within the closed region for all time. This observation is enough to indicate that a random walk process through this kind of crowded environment can be non-ergodic [44], even when ϕ is below the percolation threshold.

3. Transport of a single agent

We first consider the transport of a single agent through a crowded environment randomly populated with obstacles, to density ϕ, whose relative numbers are drawn from one of the distributions described in Section 2. After placing the obstacles on the lattice, we then place a single agent at a randomly chosen vacant site and allow it to undergo a random walk with periodic boundary conditions applied along all boundaries. To assess the effect of the different crowding environments on the transport process, we record the squared displacement of the agent, $r(t)^2 = (x(t) - x(0))^2 + (y(t) - y(0))^2$, at geometrically spaced time intervals which are related by $t_{n+1} = t_n + hg^n$, where $t_0 = 0$, $h = T(1 - g)/(1 - g^{P-1})$, P is the total number of time points and $g = 1.1$ is a geometric factor. Repeating this process for many identically prepared simulations allows us to calculate an ensemble average of $r(t)^2$.

Many previous studies have analyzed this kind of data by assuming that the mean squared displacement (MSD) follows a power law [11–14]

$$\langle r^2 \rangle = 4Dt^{\alpha}, \tag{10}$$

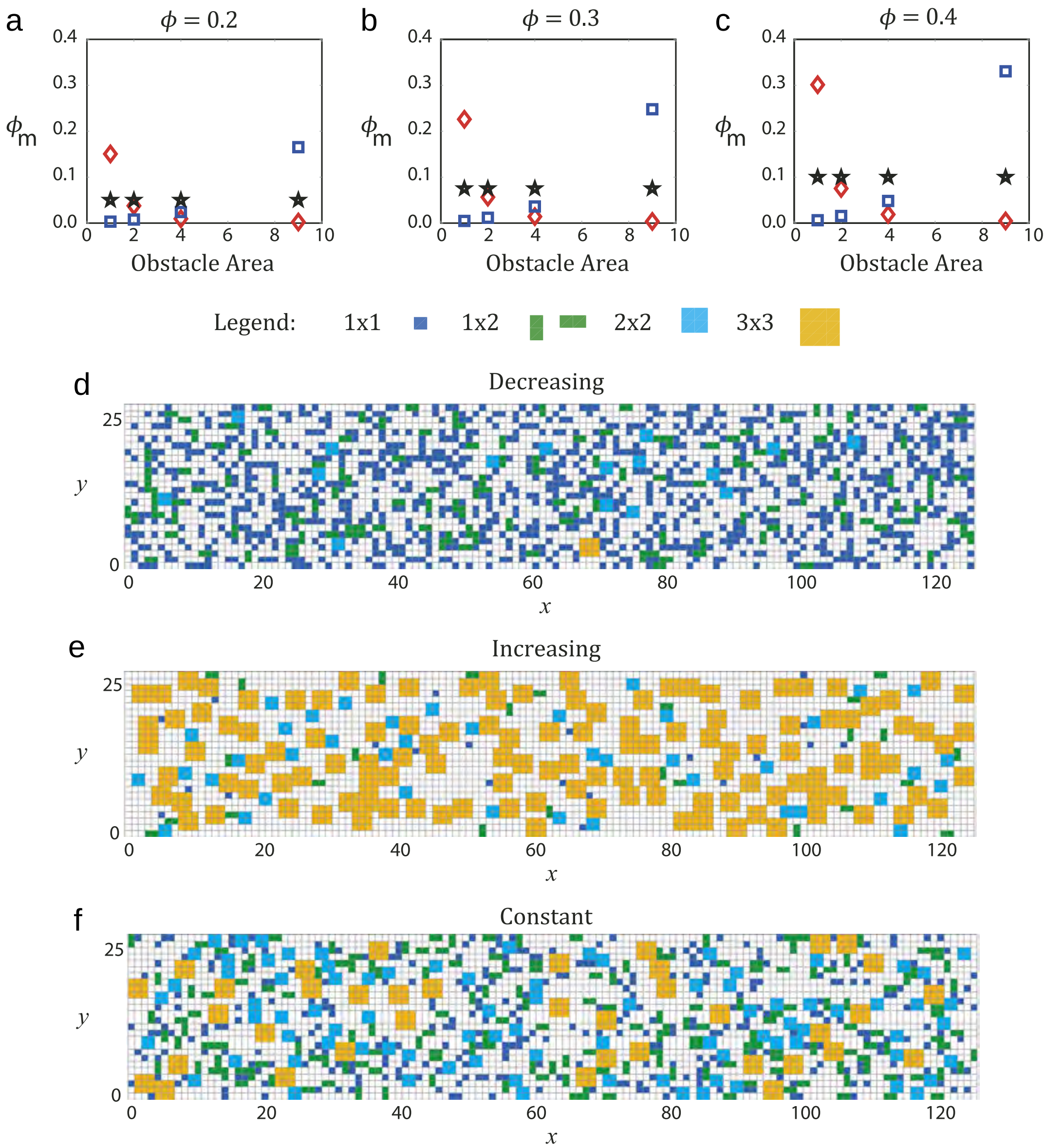

Fig. 2. (a)–(c) Density of lattice sites, ϕ_m, occupied by each type of obstacle as a function of obstacle size, for $N = 100$, $M = 100$ and $\phi = 0.2, 0.3, 0.4$, respectively. The decreasing, increasing and constant distributions are shown as red-diamond, blue-square and black-pentagrams, respectively. Images in (d)–(f) show lattice environments occupied by decreasing, increasing and constant distributions, respectively, each with $\phi = 0.4$. Each type of obstacle is uniquely colored, as described in the legend. (For interpretation of the references to color in this figure legend, the reader is referred to the web version of this article.)

where D $[L^2T^{-\alpha}]$ is a generalized diffusion coefficient, $0 < \alpha < 2$ indicates the type of transport process taking place, with $\alpha = 1$ corresponding to Fickian diffusion, $\alpha < 1$ corresponding to subdiffusion, $\alpha > 1$ corresponding to superdiffusion [26,28], and $\langle\cdot\rangle$ denotes an average over a large ensemble of simulations. In this work we focus on $0 < \alpha \leq 1$ because transport through a crowded environment is thought to be subdiffusive [26,28], whereas transport through an uncrowded environment is known to be Fickian. We rewrite Eq. (10) as $\log_{10}\left(\langle r^2\rangle/t\right) = \log_{10}(4D) + (\alpha - 1)\log_{10}(t)$, which suggests that, if the MSD follows Eq. (10), plotting $\log_{10}\left(\langle r^2\rangle/t\right)$ as a function of $\log_{10}(t)$ will lead to a straight line with slope $\alpha - 1$.

MSD data associated with a crowded environment populated by obstacles drawn from decreasing, increasing and constant distributions is shown in Fig. 3(a), (b) and (c), respectively. In each plot we include results from a control case with no obstacles present ($\phi = 0$). For this control case we see that the MSD data forms a perfectly straight line, lying on the horizontal axis, for all t considered. This observation confirms that without any obstacles present we have Fickian diffusion with $\alpha = 1$, as expected.

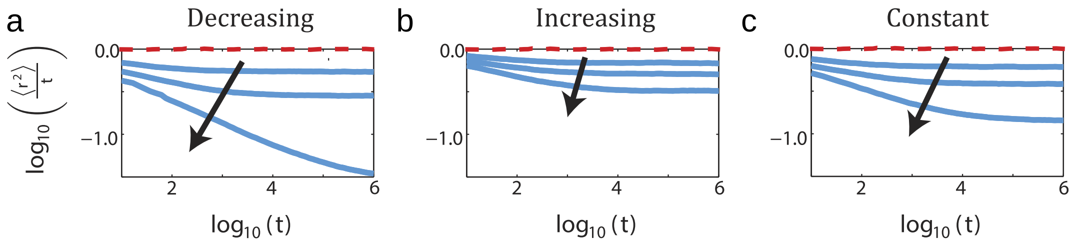

Fig. 3. (a)–(c) MSD for a single agent moving through a lattice randomly populated with obstacles whose relative densities are drawn from the decreasing, increasing, and constant distributions, respectively (solid blue). Results are also shown for the control case with no obstacles present (dashed red). In each case we have $N = M = 256$ and $\phi = 0.0, 0.2, 0.3, 0.4$. Averaged simulation data was constructed with $R = 200$ and $K = 50{,}000$. The arrow points in the direction of increasing ϕ. (For interpretation of the references to color in this figure legend, the reader is referred to the web version of this article.)

Results for the MSD data in Fig. 3 with $\phi > 0$ are more interesting. A visual, qualitative comparison of these results confirms that the details of the crowding environment have an important impact on the transport process since the curves describing the MSD are different for each obstacle distribution. To demonstrate these differences quantitatively we calculate the slope of each MSD curve in Fig. 3, for $\phi = 0.4$, at $t = 10^4$. To do this, we perform a linear regression through the five temporal intervals closest to $t = 10^4$ in each data set. The linear regression analysis provides us with an estimate of the slope from which we estimate α. This procedure gives $\alpha = 0.73$ for the decreasing distribution, $\alpha = 0.98$ for the increasing distribution and $\alpha = 0.92$ for the constant distribution, suggesting that the decreasing distribution is most effective at retarding the transport process, that the increasing distribution is least effective at retarding the transport process, and that the constant distribution is between these two extremes.

Our results for the MSD data in Fig. 3 indicate that the data does not follow the power law given by Eq. (10) when $\phi > 0$. If the MSD data were to obey this power law, the plots in Fig. 3 would be straight lines for all t. However, this is not the case, since the MSD data with $\phi > 0$ forms a family of curves. Each of these curves eventually asymptotes to a horizontal line as $t \to \infty$. This result has been observed previously by us [11] and others [12–14]. We note that there are other discrete random walk process which genuinely obey power laws, such as Eq. (10). For example, the previous stochastic model analyzed by Kehr and Kutner [45] is associated with MSD data that follows a power law with $\alpha = 1/2$. However, for the biologically motivated random walk models like we consider here, this is not the case.

4. Transport of a population of agents

The development of mathematical models that can be used to describe and predict the transport of a population of agents through a crowded environment is very important as this kind of situation is often observed and measured during biological experiments. For example, Kicheva [46] considered the motion of a population of initially confined molecules within the developing wing disc, and observed that the motion of these molecules is hindered by the presence of other biomolecules and obstacles within the wing disc. Similarly, Simpson [47] considered the motion of a population of initially confined neural crest cells along the tissues of the developing gut tissues in a chick embryo, and the motion of these cells is hindered by the presence of other cells and obstacles in the gut tissues. To mimic this kind of biological experiment we now consider a transport process in which an initially confined population of agents moves through a crowded environment. As in Section 3, we initially populate the lattice with obstacles drawn from an increasing, decreasing or constant distribution to density ϕ. To initialize the simulation, we populate all vacant lattice sites in the vertical columns for which $(L_x - w) \le 2x \le (L_x + w)$ with agents. This corresponds to a population of agents initially confined to a vertical strip, of width w, located at the center of the domain. We then allow the agents to undergo an unbiased nearest neighbor random walk in which we enforce a straightforward exclusion mechanism by aborting potential motility events which would lead to an agent occupying the same lattice site as another agent or an obstacle. Absorbing boundary conditions are applied at $x = 0$ and $x = L_x$, and periodic boundary conditions are applied along $y = 0$ and $y = L_y$.

Fig. 4(a), (d) and (g) shows a lattice which has been stochastically populated with obstacles from the decreasing, increasing and constant distributions, respectively, with $\phi = 0.4$. In Fig. 4(b), (e) and (h) we show the same lattices as in Fig. 4(a), (d) and (g), except that now we have placed a population of agents onto all vacant sites in the central 21 columns. We treat the system shown in Fig. 4(b), (e) and (h) as the initial condition for our simulations describing the transport of a population of agents through a crowded environment. In Fig. 4(c), (f) and (i), we show the resulting distribution of agents from a single realization at $T = 1000$. One way of comparing the distribution of agents in Fig. 4(c), (f) and (i) is to measure the width of the spreading population of agents. Recalling that the width of the initial distribution of agents was 21 lattice sites at $t = 0$, by $t = 1000$ the widths of the spreading population are 61, 77 and 75 lattice sites for the decreasing, increasing and constant distributions, respectively. These differences suggest that the rate at which the initially confined population of agents is able to spread through the crowded environment is greatest for the environment populated by obstacles from the increasing distribution, and smallest when the obstacles are drawn from the decreasing distribution. This trend is consistent with the results described in Section 3 for the motion of a single agent. Since we have only dealt with a single realization of the stochastic model to arrive at these preliminary observations, we now consider performing many identically prepared

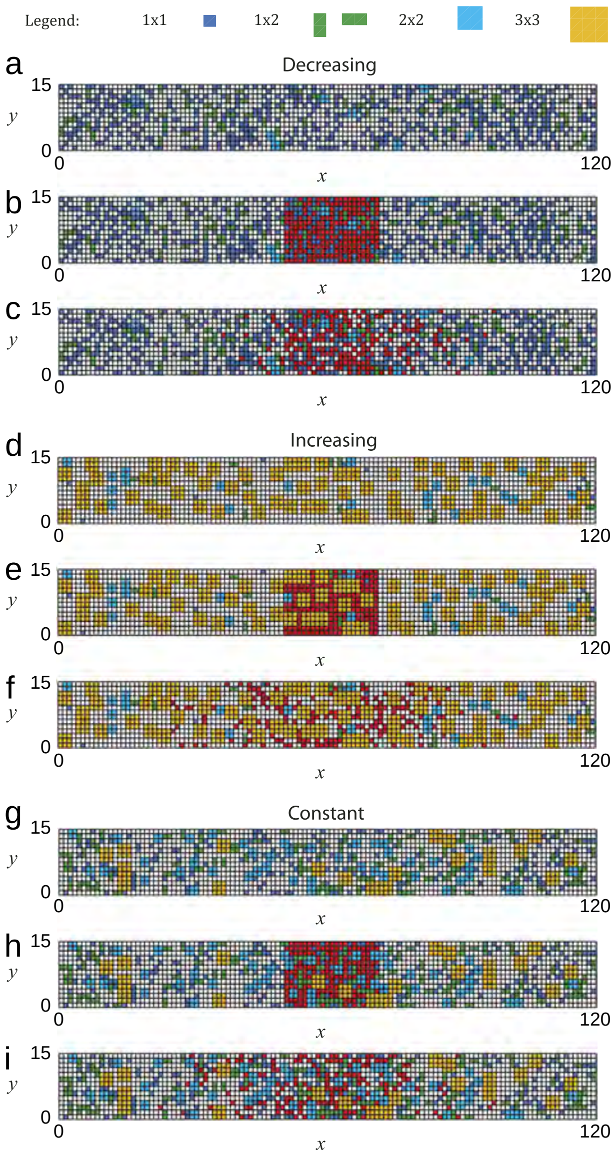

Fig. 4. Results in (a)–(c); (d)–(f) and (g)–(i) show a lattice occupied by a decreasing, increasing and constant distribution of obstacles, respectively. Each type of obstacle is uniquely colored, as described in the legend. Results in (a), (d) and (g) show the lattice occupied by the obstacles without any agents present, each with $\phi = 0.40$. Results in (b), (e) and (h) show the same lattice and obstacle distribution where the vacant sites within the central 21 columns of the lattice have been initialized with motile agents. Results in (c), (f) and (i) show the distribution of agents after performing a random walk simulation until $T = 1000$. All results correspond to $M = 120$, $N = 15$ and $w = 21$. (For interpretation of the references to color in this figure legend, the reader is referred to the web version of this article.)

realizations to investigate whether similar differences occur when we describe the process using averaged data. To ensure that we do not encounter the Fickian regime we consider two observation times, $T = 1000$ and $T = 3000$, as our MSD simulations suggest that the transition from non-Fickian to Fickian behavior occurs after $T = 10^4$ for all situations with $\phi > 0$ that we consider.

Since our initial distribution of agents in Fig. 4 is, on average, independent of vertical position, we can characterize the averaged transport process as a function of the horizontal coordinate, x, and time, t [48,49]. We construct averaged agent population density data in the following way: once the simulation reaches time T we calculate the density of agents in each vertical column of the lattice. Let $n_k(i, j)$ denote the occupancy of site (i, j) during the kth identically prepared realization such that $n_k(i, j) = 0$ corresponds to a vacant site and $n_k(i, j) = 1$ corresponds to a site which is occupied by an agent. The density of agents in each vertical column is $\left[\sum_{j=1}^{M} n_k(i, j)\right] / \bar{n}_k$, where we have normalized the density by dividing by the number of agents which initially occupy the central column at $x = L_x/2$, $\bar{n}_k = \sum_{j=1}^{M} n_k(L_x/2, j)$. The average density of agents in each column, at time T, further averaged using data from K identically prepared realizations, is given

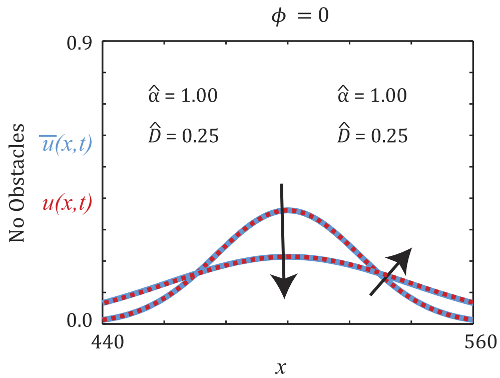

Fig. 5. Evolution of the average population density, $\bar{u}(x, t)$ (blue), and the least squares solution of Eq. (12), $u(x, t)$ (red-dashed). Results show density profiles for $\phi = 0$ and correspond to two different simulation times, $T = 1000$ and $T = 3000$, with the arrows indicating the direction of increasing time. The least squares estimates $\hat{\alpha}$ and $\hat{D}$ are given in the top left of the figure for $T = 1000$, and in the top right of the figure for $T = 3000$. Simulation parameters correspond to $N = 100$, $M = 1000$ and $w = 21$, with $R = 100$ and $K = 100{,}000$. The Fourier series solution for $u(x, t)$ was obtained by truncating the infinite series, Eq. (13), after 30,000 terms. (For interpretation of the references to color in this figure legend, the reader is referred to the web version of this article.)

by [48,49]

$$\bar{u}(x, T) = \frac{1}{K}\sum_{k=1}^{K}\left(\frac{1}{\bar{n}_k}\sum_{j=1}^{M} n_k(i, j)\right). \tag{11}$$

It has become increasingly common for researchers to implicitly represent transport through crowded environments using FDE models [19–26,28], and we note that many of these previous applications neglect to consider the relationship between the FDE description and the underlying stochastic mechanism. To improve our understanding of whether averaged density data from our relatively straightforward stochastic model can be accurately represented by an FDE framework, we now attempt to match our averaged agent density information, $\bar{u}(x, T)$, with the solution of

$$\frac{\partial^\alpha u}{\partial t^\alpha} = D\frac{\partial^2 u}{\partial x^2}, \quad 0 < x < L_x, \tag{12}$$

where $\partial^\alpha/\partial t^\alpha$ denotes a Caputo fractional derivative [50] of order α and L_x is the length of the spatial domain. Appropriate boundary and initial conditions that match our stochastic simulations are $u(0, t) = 0$, $u(L_x, t) = 0$ and $u(x, 0) = \mathrm{H}(x - [L_x - w]/2) - \mathrm{H}(x - [L_x + w]/2)$, where $\mathrm{H}(\cdot)$ is the Heaviside function. For these conditions the solution of Eq. (12) is

$$u(x, t) = \sum_{\kappa=1}^{\infty} A_\kappa \sin\left(\frac{\kappa\pi x}{L_x}\right) \mathrm{E}_\alpha\left[-D\left(\frac{\kappa\pi}{L_x}\right)^2 t^\alpha\right], \tag{13}$$

where $\mathrm{E}_\alpha[\cdot]$ denotes a Mittag-Leffler function [50], and $A_\kappa = 4\{\sin[\kappa\pi/2]\sin[\kappa\pi w/(2L_x)]\}/(\kappa\pi)$.

To investigate whether Eq. (12) provides an accurate framework to describe our averaged density data we must determine appropriate values of D and α. We estimate D and α by matching $u(x, t)$ to the averaged agent population density, $\bar{u}(x, t)$, using the Levenberg–Marquardt algorithm [51]. To apply this algorithm we first define $\epsilon_i = \bar{u}(x, T) - u(x, T)$, which measures the difference between the observed averaged data and the solution of Eq. (12) at $t = T$. The Levenberg–Marquardt algorithm minimizes $\mathcal{S}(\alpha, D) = \sum_{i=0}^{M} \epsilon_i^2$, where the sum is taken over all vertical columns of the lattice, by iteratively stepping from an initial guess, (α_0, D_0), down the gradient of $\mathcal{S}(\alpha, D)$ to the least squares estimate, $(\hat{\alpha}, \hat{D})$. As the algorithm proceeds we always ensure that $0 < D \leq 1/4$ and $0 < \alpha \leq 1$, as solutions outside of this parameter range are physically unrealistic for our calculations on a two-dimensional lattice with unit lattice spacing. Furthermore, we always test that our estimates of $(\hat{\alpha}, \hat{D})$ are independent of the initial guess, (α_0, D_0).

We first consider a control case with no obstacles ($\phi = 0$). Results are shown in Fig. 5, confirming that the match between the density profiles from the averaged stochastic data and the solution of the Eq. (12) with the least squares parameter estimates, $(\hat{\alpha}, \hat{D})$ is excellent. Furthermore, the Levenberg–Marquardt algorithm shows that we have $\hat{\alpha} = 1.00$ and $\hat{D} = 0.25$ at both $T = 1000$ and $T = 3000$. This is an expected result since there are no obstacles on the lattice and previous research has shown, from a theoretical point of view, that averaged density data associated with this random walk model without obstacles is governed by Eq. (12) with $\alpha = 1$ and $D = 1/4$ [48,49]. In this case Eq. (12) reduces to the linear diffusion equation. For our study it is relevant to make note of the fact that we obtain the same estimates of $\hat{\alpha} = 1.00$ and $\hat{D} = 0.25$ at two different inspection times, $T = 1000$ and $T = 3000$.

Results in Fig. 6 show that the averaged agent population density, $\bar{u}(x, t)$, superimposed on the solution of Eq. (12), $u(x, t)$, is obtained using the least squares parameter estimates, $(\hat{\alpha}, \hat{D})$, for $\phi > 0$. Several observations can be made

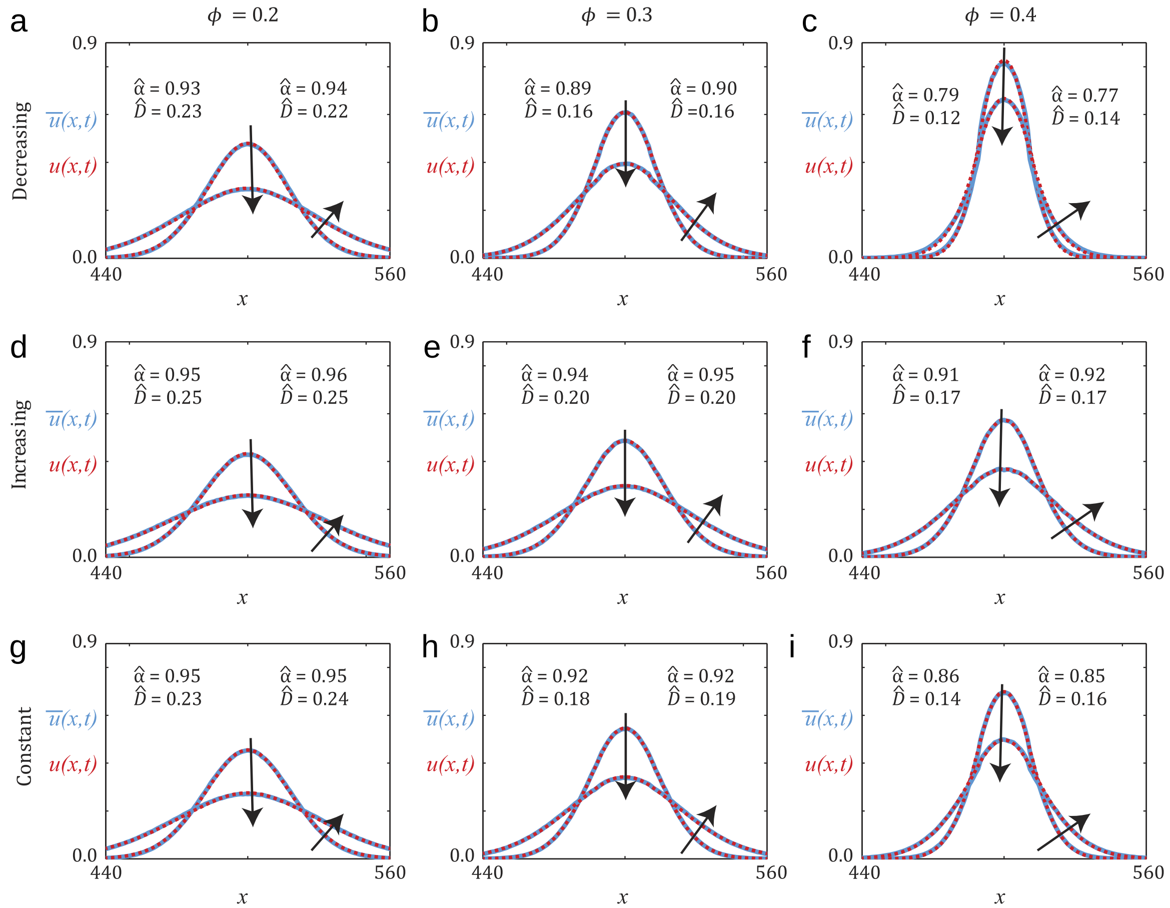

Fig. 6. Evolution of the average population density, $\bar{u}(x, t)$ (blue), and the least squares solution of Eq. (12), $u(x, t)$ (red-dashed). Results in (a)–(c); (d)–(f) and (g)–(i) correspond to decreasing, increasing and constant obstacle distributions, respectively. Results in (a), (d), (g); (b), (e), (h) and (c), (f), (i) show density profiles for $\phi = 0.2, 0.3, 0.4$, respectively. Results in each subfigure correspond to two different simulation times, $T = 1000$ and $T = 3000$, with the arrows indicating the direction of increasing time. The least squares estimates $\hat{\alpha}$ and $\hat{D}$ are given in the top left of each subfigure for $T = 1000$, and in the top right of each figure for $T = 3000$. Simulation parameters correspond to $N = 100$, $M = 1000$ and $w = 21$, with $R = 100$ and $K = 100,000$. The Fourier series solution for $u(x, t)$ was obtained by truncating the infinite series, Eq. (13), after 30,000 terms. (For interpretation of the references to color in this figure legend, the reader is referred to the web version of this article.)

from the results in Fig. 6. Firstly, the match between the averaged agent density data and the solution of Eq. (12) with $(\hat{\alpha}, \hat{D})$ is excellent. However, our estimates of $\hat{D}$ and $\hat{\alpha}$ are very sensitive to the different types of obstacle distributions. For example, at $T = 1000$ with $\phi = 0.4$, we have $\hat{\alpha} = 0.79, 0.91$ and 0.86 for the decreasing, increasing and constant obstacle distributions, respectively. This suggests that the decreasing distribution is very effective at retarding the transport process, that the increasing distribution is least effective at retarding the transport process, and that the constant distribution lies between these two cases. Secondly, unlike the control case with $\phi = 0$, the calibration procedure for the data with $\phi > 0$ indicates that our estimates of $\hat{D}$ and $\hat{\alpha}$ depend upon the inspection time, T. This observation is contrary to the assumptions underpinning Eq. (12), where D and α are supposed to be constant.

5. Discussion

In this work, we consider a transport process through a crowded environment that is populated by immobile obstacles of varying size and shape. In particular, we focus on three distributions of obstacle size and shape which represent an environment crowded by the following: a relative abundance of small obstacles; a relative abundance of large obstacles; and an intermediate case. This framework allows us to create qualitatively different crowded environments whilst holding the density of occupied lattice sites constant, and to explore how the details of the distribution of agent shape and size impacts the transport properties.

We first consider the motion of a single motile agent and record the MSD as a function of time. To analyze these data, we use a standard method [11–15] and plot $\log_{10}\left(\langle r^2\rangle/t\right)$ as a function of $\log_{10}(t)$. If the MSD was to follow a power law, these data would fall on a straight line. Instead, we observe that these data do not fall on a straight line, indicating that the transport process does not follow Eq. (10). This kind of observation is consistent with several previous studies [12–15]. To quantify how the transport process is affected by different distributions of obstacle shapes and sizes, we follow a standard approach and estimate the slope of the plot of $\log_{10}\left(\langle r^2\rangle/t\right)$ as a function of $\log_{10}(t)$. These results confirm that the details of the distribution of the obstacles can play an important role, since different distributions with the same value of ϕ lead to very different MSD data.

To extend our analysis to apply to biological experiments that involve the motion of populations of cells or molecules, we also consider the motion of a population of motile agents through various crowded environments. To simplify our analysis, we choose an initial condition that is, on average, symmetric in the vertical direction and recorded average density of agents in each column of the lattice. This framework allows us to describe the transport of a population of agents as a function of the horizontal coordinate, x, and time, t. Extracting averaged density data from our stochastic model confirms that the details of the distribution of obstacle size and shape have an important impact on the transport process, since we observe that otherwise identical populations of agents are able to move through some environments far more easily than others, even though the density of obstacles, ϕ, is the same.

To provide quantitative insight into our results describing the transport of a population of agents, we match our averaged density data with the solution of a standard FDE model, Eq. (12), to provide a least squares estimate of D and α for the various crowding environments. Our results confirm that α decreases with ϕ, as expected, with the additional result that α also decreases when we consider distributions of obstacles in which small obstacles dominate. This trend is consistent with the MSD data, and together our observations confirm that obstacle distributions in which smaller obstacles dominate are more effective at retarding the transport process [52]. These outcomes imply that if we are to reliably predict and model transport through a crowded environment, we must characterize both the total density of obstacles, ϕ, as well as additional details of the distribution of obstacle shapes and sizes.

We conclude with some cautionary remarks. A fundamental assumption underlying the use of FDE models is that D and α are constants that do not depend on time. Since our least squares estimates of D and α in Eq. (12) appear to depend on the inspection time, T, our results suggest that FDE models ought to be used with great care. Despite the widespread use of FDE models like Eq. (12), our model calibration procedure implies that even the relatively straightforward random walk process we consider here cannot be properly described using this kind of FDE model. Our observation that the averaged density profiles are not described by Eq. (12) is consistent with our analysis of MSD data which do not follow the commonly invoked power law, Eq. (10).

Acknowledgments

We appreciate support from the Australian Research Council (DP140100249, FT130100148). Computational resources used in this work were provided by the High Performance Computing and Research Support Group at Queensland University of Technology. We thank the anonymous reviewers for their helpful comments and suggestions.

References

[1] M. Weiss, M. Elsner, F. Kartberg, T. Nilsson, Biophys. J. 87 (2004) 3518.
[2] M. Weiss, Crowding, diffusion and biochemical reactions, in: International Review of Cell and Molecular Biology, Elsevier, 2014, (Chapter 11).
[3] M. Saxton, Biophys. J. 103 (2012) 2411.
[4] F. Höfling, T. Franosch, Rep. Progr. Phys. 76 (2013) 046602.
[5] R.J. Ellis, Trends Biochem. Sci. 26 (2001) 297.
[6] J.A. Dix, A. Verkman, Annu. Rev. Biophys. 37 (2008) 247.
[7] J. Mittal, J.R. Errington, T.M. Truskett, Phys. Rev. E 74 (2006) 040102.
[8] M. Ganjeh-Ghazvini, M. Masihi, M. Ghaedi, Physica A 406 (2014) 214.
[9] M.A.A. Silva, G.M. Viswanathan, J.C. Cressoni, Physica A 421 (2015) 522.
[10] D.V. Nicolau Jr., J.F. Hancock, K. Burrage, Biophys. J. 92 (2007) 1975.
[11] A.J. Ellery, M.J. Simpson, S.W. McCue, R.E. Baker, J. Chem. Phys. 140 (2014) 054108.
[12] M.J. Saxton, Biophys. J. 66 (1994) 394.
[13] M.J. Saxton, Biophys. J. 72 (1997) 1744.
[14] E. Vilaseca, A. Isvoran, S. Madurga, I. Pastor, J. Garcés, F. Mas, Phys. Chem. Chem. Phys. 13 (2011) 7396.
[15] A. Isvoran, E. Vilaseca, L. Unipan, J. Garcés, F. Mas, Rev. Roum. Chim. 53 (2008) 415.
[16] A. Wedemeier, H. Merlitz, C.-X. Wu, J. Langowski, J. Chem. Phys. 127 (2007) 045102.
[17] A. Wedemeier, H. Merlitz, J. Langowski, Europhys. Lett. 88 (2009) 38004.
[18] T. Bauer, F. Höfling, T. Munk, E. Frey, T. Franosch, Eur. Phys. J. Spec. Top. 189 (2010) 103.
[19] M.M. Meerschaert, P. Straka, J. Stat. Phys. 149 (2012) 878.
[20] M.M. Meerschaert, P. Straka, Math. Model. Nat. Phenom. 8 (2013) 1.
[21] P. Straka, B.I. Henry, Stochastic Process. Appl. 121 (2011) 325.
[22] S.B. Yuste, L. Acedo, K. Lindenberg, Phys. Rev. E 69 (2004) 036126.
[23] S.B. Yuste, K. Lindenberg, Phys. Rev. Lett. 87 (2001) 118301.
[24] E. Abad, S.B. Yuste, K. Lindenberg, Phys. Rev. E 81 (2010) 031115.
[25] B. Henry, T. Langlands, S. Wearne, Phys. Rev. E 74 (2006) 031116.
[26] R. Metzler, J. Klafter, Phys. Rep. 399 (2000) 1.
[27] J. Gajda, A. Wyłomańska, Physica A 405 (2014) 104.
[28] I.M. Sokolov, J. Klafter, A. Blumen, Phys. Today 55 (2002) 48.
[29] M.M. Meerschaert, D.A. Benson, H.-P. Scheffler, B. Baeumer, Phys. Rev. E 65 (2002) 041103.
[30] H.W. Cho, G. Kwon, B.J. Sung, A. Yethiraj, Phys. Rev. Lett. 109 (2012) 155901.
[31] T. Ando, J. Skolnick, PNAS 107 (2010) 18457.

[32] S.R. McGuffee, A.H. Elcock, PLoS Comput. Biol. 6 (3) (2010) e1000694.
[33] M.J. Skaug, R. Faller, M.L. Longo, J. Chem. Phys. 134 (2011) 215101.
[34] A.A. Like, W.L. Chick, Diabetologia 6 (1970) 216.
[35] B.J. Sung, A. Yethiraj, Phys. Rev. Lett. 96 (2006) 228103.
[36] F. Höfling, T. Munk, E. Frey, T. Franosch, J. Chem. Phys. 128 (2008) 164517.
[37] M. Cieśla, E. Gudowska-Nowak, F. Sagués, I.M. Sokolov, J. Chem. Phys. 140 (2014) 044706.
[38] C. Scholz, F. Wirner, J. Götz, U. Rüde, G.E. Schröder-Turk, K. Mecke, C. Bechinger, Phys. Rev. Lett. 109 (2012) 264504.
[39] K. Murase, T. Fujiwara, Y. Umemura, K. Suzuki, R. Iino, H. Yamashita, M. Saito, H. Murakoshi, K. Ritchie, A. Kusumi, Biophys. J. 86 (2004) 4075.
[40] I.M. Sokolov, Soft Matter 8 (2012) 9043.
[41] T.M. Liggett, Interacting Particle Systems, Springer, 2005.
[42] D.T. Gillespie, J. Phys. Chem. 81 (1977) 2340.
[43] T. Andreescu, An Introduction to Diophantine Equations: A Problem-Based Approach, Birkhauser, 2010.
[44] M. Magdziarz, A. Weron, Phys. Rev. E 84 (2011) 051138.
[45] K.W. Kehr, R. Kutner, Phys. 110A (1982) 535.
[46] A. Kicheva, P. Pantazis, T. Bollenbach, Y. Kalaidzidis, T. Bittig, F. Jülicher, M. González-Gaitán, Science 315 (2007) 521.
[47] M.J. Simpson, D.C. Zhang, M. Mariani, K.A. Landman, D.F. Newgreen, Dev. Biol. 302 (2007) 553.
[48] M.J. Simpson, K.A. Landman, B.D. Hughes, Physica A 388 (2009) 399.
[49] M.J. Simpson, K.A. Landman, B.D. Hughes, Phys. Rev. E 79 (2009) 031920.
[50] I. Podlubny, Fractional Differential Equations, Elsevier Science, 1998.
[51] K. Levenberg, Quart. Appl. Math. 2 (1944) 164.
[52] K.A. Sharp, PNAS 112 (2015) 7990.